3-7-2008

Hysteresis of ultrasmall Fe–Pt particles

Ralph Skomski
University of Nebraska-Lincoln, rskomski2@unl.edu

J. Ping Liu
University of Texas, Arlington, pliu@uta.edu

C. B. Rong
University of Texas at Arlington

David J. Sellmyer
University of Nebraska-Lincoln, dsellmyer@unl.edu

Hysteresis of ultrasmall Fe–Pt particles

Ralph Skomski,[1,a)] J. P. Liu,[2] C. B. Rong,[2] and D. J. Sellmyer[1]
[1]*Physics and Astronomy and Nebraska Center for Materials and Nanoscience, University of Nebraska, Lincoln, Nebraska 68588, USA*
[2]*Department of Physics, University of Texas, Arlington, Texas 76019, USA*

(Presented on 6 November 2007; received 11 September 2007; accepted 14 November 2007; published online 7 March 2008)

The magnetization reversal in very small FePt particles is investigated by analytical and numerical calculations. The modeling focuses on particles with diameters from 3 to 15 nm, as produced by a salt-matrix annealing technique. Experiment shows that the particles exhibit a certain degree of structural inhomogenity, which has a far-reaching effect on the magnetic hysteresis. In particles larger than about 10 nm, the magnetization-reversal mode is strongly inhomogeneous, and there are several scenarios that depend on the symmetry of inhomogenity. Small particles reverse nearly coherently, and the coercivity is essentially equal to the volume-averaged anisotropy. In this case, nonrectangular hysteresis loops reflect factors such as grain misalignment, particle-size distribution, and different degrees of $L1_0$ order in different particles. © *2008 American Institute of Physics*. [DOI: 10.1063/1.2837623]

The high magnetic anisotropy and corrosion resistance make $L1_0$-ordered FePt ideal for the next generations of magnetic recording media and advanced permanent magnets.[1–7] Recently, a salt-annealing method has been used to produce nearly monodisperse $L1_0$ nanoparticles with stable room-temperature magnetism down to sizes of 3 nm.[8] Smaller particles ($D \sim 2$ nm) remain in the disordered face-centered-cubic (fcc) phase, and there is probably some transition region with incomplete or inhomogeneous $L1_0$ ordering even after annealing.[8–10] Due to low magnetic anisotropy and reduced particle size, small particles ($D \sim 2$ nm) are superparamagnetic at room temperature.

Magnetic hysteresis is an involved phenomenon, and the magnetization reversal in $L1_0$ nanostructures is only partially understood. Hysteresis loops encountered in practice are often nonrectangular, and observed coercivities are generally smaller than the Stoner–Wohlfarth predictions. To a large extent, this reflects incomplete c-axis alignment, both the random orientation of the particles in the sample and inside the particles. Very small particles exhibit some additional smoothing due to thermal activation, but even for aligned single-crystalline particles at zero temperature there remains some smoothing due to structural imperfections, such as incomplete $L1_0$ ordering near the surface.[11,12]

In this paper, we do not attempt a full coercivity analysis, which would require a detailed knowledge of the nanocrystalline structure, most notably the local easy-axis direction and the local anisotropy constant K_u, but focus on the role of imperfections in the core of the particle and at the surface.

FePt nanoparticles having fcc structure and diameters from 3 to 15 nm were prepared via chemical reduction of $Pt(acac)_2$ and thermal decomposition of $Fe(CO)_5$ in the presence of oleic acid and oleyl amine. The fcc nanoparticles were then transformed to $L1_0$ nanoparticles with no particle growth using the salt-matrix annealing technique with salt/sample mass ratio around 400:1.[13] The heat treatments were carried out at 700 °C for 4 h which is considered sufficient for the ordering phase transition. The morphology and crystalline structure were characterized by transmission electron microscopy (TEM), selected area electron diffraction (SAED), and x-ray diffraction (XRD), and the nominal composition of the nanoparticles is about $Fe_{54}Pt_{46}$. The hysteresis loops were measured with a magnetic properties measurement system from specimens that were a mixture of epoxy and the magnetic nanoparticles.[9]

Figure 1 shows high-resolution TEM images of 3 and 8 nm FePt nanoparticles after annealing in a salt matrix at 700 °C for 4 h. It was found that the separating media (salt and surfactants) conserve the particle sizes during annealing. The standard deviation of the nanoparticle diameters is about 10%, based on particle-number averages obtained from the high-resolution TEM images. XRD and SAED patterns confirm the phase transformation from fcc FePt to $L1_0$-ordered FePt; details about the crystal structure of the alloys have been published elsewhere.[8,9]

Figure 2 shows room-temperature hysteresis loops for different particles sizes. The saturation magnetization in-

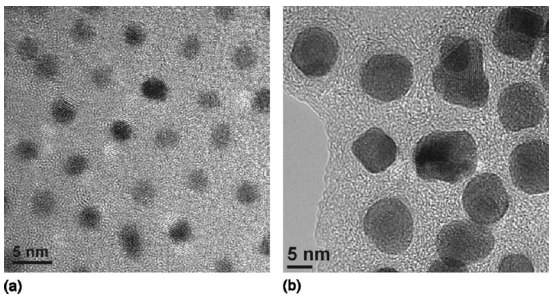

FIG. 1. TEM image of FePt nanoparticles having diameters of (a) 3 nm and (b) 8 nm.

a)Electronic mail: rskomski@neb.rr.com.

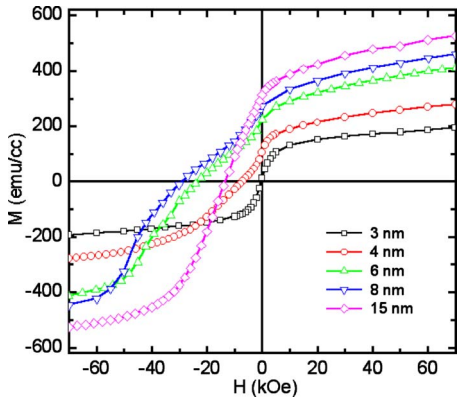

FIG. 2. (Color online) Hysteresis loops of FePt particles of different sizes.

creases monotonously with increasing particle size, whereas the coercivity reaches a maximum at a particle size of 8 nm. The increase of coercivity for the 3–8 nm particles reflects the improved chemical ordering ($L1_0$ order parameter), which translates into an enhancement of the magnetocrystalline anisotropy. The decrease of the coercivity for large particle sizes is of micromagnetic origin, associated with real-structure imperfections such as polycrystallinity and reduced anisotropy at the surface (see below).

Since we are primarily interested in the effect of imperfections, as contrasted to the magnitude and direction of the average anisotropy, we assume that the particles are c-axis aligned along the direction of the field $\mathbf{H}=H\mathbf{e}_z$. Starting from saturation, $\mathbf{M}=M_s\mathbf{e}_z$, nucleation involves a small magnetization component $\mathbf{M}_{\text{nucl}}=M_s\mathbf{m}$, where $\mathbf{m}=m_x\mathbf{e}_x+m_y\mathbf{e}_y$.[14,15] The components m_x and m_y are degenerate in fair approximation, so that we can restrict ourselves to the consideration of $m=|\mathbf{m}|$.[15] As elaborated elsewhere,[15,16] the nucleation modes obey the partial differential equation,

$$-A\nabla^2 m+[K(\mathbf{r})-\mu_0 M_s H/2]m=0, \tag{1}$$

where the lowest-order uniaxial anisotropy constant $K(\mathbf{r})$ describes the real or defect structure of the magnet. (For homogeneous particles, $K(r)=\langle K\rangle$, Eq. (1) reproduces coherent rotation, irrespective of domain-wall width and particle size.) In Eq. (1), the magnetostatic interaction is incorporated into K (shape anisotropy) and H (interaction field). We also make the approximation $H(\mathbf{r})=H_{\text{ext}}-DM$, that is, the magnetostatic self-interaction is described by a demagnetizing factor. This is reasonable because the particles are nearly spherical and magnetically hard. It has also been shown that exchange inhomogenities $A(\mathbf{r})$ have a relatively small effect on the hysteresis.[15]

There are exact solutions of Eq. (1) for a number of planar[18] and three-dimensional[16,17] cases, but all calculations require an explicit knowledge of the "defect structure" $K(\mathbf{r})$. What can we conclude about the nucleation mode from the symmetry of the grain imperfection, without explicit knowledge of $K_1(\mathbf{r})$? Some cases frequently encountered in practice are reduced surface or interface anisotropy, defects localized at grain or particle surfaces, and bulk defects.[15,18]

To treat the problem perturbatively, we start from a homogeneous system where Eq. (1) assumes the form $-\nabla^2 m-k^2 m=0$ and, in spherical coordinates,

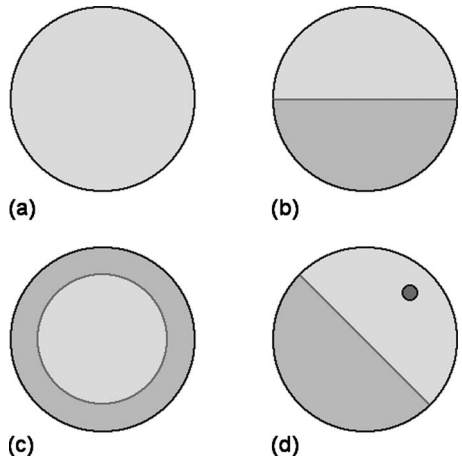

FIG. 3. Nucleation modes in spherical particles: (a) coherent rotation, (b) example of a low-lying asymmetric excited mode, (c) lowest-lying symmetric excited mode, and (d) typical situation in practice. Bright and dark regions denote magnetization components perpendicular magnetization components of opposite directions, and the small dot in (d) is a structural imperfection.

$$-\frac{d^2m}{dr^2}-\frac{2}{r}\frac{dm}{dr}+\frac{j(j+1)}{r^2}m-k^2m^2=0. \tag{2}$$

Interpretation of Eq. (2) as a Schrödinger equation reveals that j has the character of an angular quantum number. For example, $j=0$ corresponds to s-type state (spherical symmetry), whereas $j=1$ describes p-state configurations with $m(-\mathbf{r})=-m(\mathbf{r})$. As well known in magnetic resonance, the solutions of Eq. (2) are spherical Bessel functions $J_{j+1/2}(kr)$ or $j_j(kr)$. However, in contrast to magnetic resonance, we are not interested in the excited modes themselves but in the effect of excited modes on the lowest-lying or nucleation mode. In other words, we ask ourselves how the nucleation mode differs from coherent rotation.

The functions are subject to the boundary condition $dm/dr=0$ at $r=R$ because nonzero gradients dm/dr at the particle surface correspond to an unphysical exchange-energy enhancement at the surface. From $j_0(x)=\sin(x)/x$ and $j_1(x)=\sin(x)/x^2-\cos(x)/x$,[19] we find the lowest-lying modes $dj_0/dx=0$ at $x=0$ and $x=4.493\,41$, and $dj_1(x)/dx=2.081\,58$. In the quantum-mechanical analogy, the modes with $k=0$, $k=4.493\,41/R$, and $k=2.081\,58$ have the respective symmetries of $1s$, $2s$, and $2p$ states, and the corresponding excitation fields are given by

$$H=2K/\mu_0 M_s+2Ak^2/\mu_0 M_s. \tag{3}$$

Figure 3 shows the small magnetization components $m(\mathbf{r})=m_x(\mathbf{r})$ for these modes. Bright and dark regions correspond to positive and negative $m(\mathbf{r})$, respectively. For example, Fig. 3(c) means that the nucleation starts from the surface of the particle. There are three modes or "orbitals" with $j=1$, corresponding to quantum-mechanical $|p_x\rangle$, $|p_y\rangle$, and $|p_z\rangle$ orbitals. Figure 3(b) shows the $|y\rangle$ orbital, but in reality, the modes hybridize. For example, the mode in Fig. 3(d) is of the type $|x\rangle+|y\rangle$. Note that the mode $|z\rangle$ means $m_x(\mathbf{r})\sim z/r$, rather than describing M_z.

In small particles, the lowest-lying mode is uniform [Fig. 3(a)] because k in Eq. (3) scales as $1/R$. However, there is

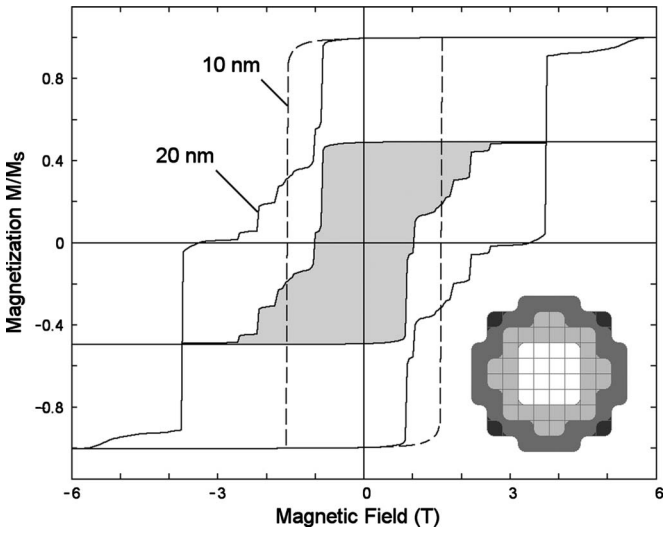

FIG. 4. Simulated loops. The gray area is the magnetization of the shell of the 20 nm particle. The small "jumps" in the loop mean that groups of cells switch in a coordinated manner. The jumps depend on the cell size and can be shown to smooth on ensemble averaging.

generally some admixture of "excited" states $|e\rangle$, meaning that the reversal mode is only approximately coherent. The symmetry of $|e\rangle$ depends on the defect structure $K(\mathbf{r})$. Asymmetric defects, such as the dark circle shown in Fig. 3(d), involve a superposition of degenerate p-type modes $|e\rangle=|p\rangle$, which is then admixed to the uniform mode by $\langle 0|K|p\rangle = (3/4\pi R^3)\int s_0(\mathbf{r})K(\mathbf{r})p(\mathbf{r})dV$. The lowest-lying nonuniform symmetric mode $s_1(\mathbf{r})$ or $|e\rangle=|1\rangle$, shown in Fig. 3(c), is more difficult to admix because it has a relatively large k. However, $\langle 0|K|1\rangle=(3/4\pi R^3)\int s_0(\mathbf{r})K(\mathbf{r})s_1(\mathbf{r})dV$ may be quite large for inhomogenities located at the particle surface, while $\langle 0|K|p\rangle=0$ by symmetry.

Perturbation theory yields the nucleation field

$$H_n = \frac{2\langle K\rangle}{\mu_0 M_s} - \frac{2|\langle e|K|0\rangle|^2}{\mu_0 M_s A k^2}. \tag{4}$$

Consider, for example, a thin shell of reduced anisotropy (shell thickness Δ). The reduction in the average $\langle K\rangle$ is proportional to Δ, whereas the reduction in the second term scales as Δ^2. The second term is therefore a small correction unless k is small (or R is large).

To investigate the magnetization reversal numerically, we have performed calculations using a C++ spin-relaxation code with built-in monitoring of subsystem magnetizations. Figure 4 shows the results of a typical systems. In the figure, the nanoparticle is divided into 552 numerical cells, as shown in the inset. To model the real structure, we have assumed a shell of reduced anisotropy. The respective shell thicknesses are 1 and 2 nm for the 10 and 20 nm particles, meaning that the shells occupy about half the particle volume in both cases.

The average anisotropy is assumed to be about 3.3 $\mathrm{MJ/m^3}$, that is, about 50% of the anisotropy $K_{\max}$ of fully ordered FePt. However, the anisotropy is unevenly distributed: the core has $0.75K_{\max}$, whereas the shell has only $0.25K_{\max}$. The particle with $D=20$ nm exhibits a pronounced magnetization inhomogenity during switching, as can be seen by comparing the shell magnetization (gray) with the full loop. By contrast, for 10 nm particles, the core-shell particle has nearly the same hysteresis loop as a homogeneous particle with $K=0.5K_{\max}$. Equation (4) contains a k^2 dependence of the magnetic field, meaning that anisotropy-field difference is enhanced by a factor of 4 if the feature size doubles.

In conclusion, we have investigated the origin and realization of hysteresis in small FePt nanoparticles. In lowest-order theory, applicable to very small particles ($D=3$ to about 10 nm), the coercivity is given by the particles' average anisotropy, irrespective of the geometry of the imperfection but including the particle-size dependence of the anisotropy. In particles larger than 10 nm, there is a clear distinction between imperfections nearly symmetrically distributed over the particle's surface and localized defects. The analysis of the involved spherical Bessel functions reveals that the surface modes have a relatively high energy but are often easily excited by typical defects, due to the large fraction of surface atoms, and the same picture is reproduced by numerical simulations.

This research is supported at Nebraska by DOE and NCMN, and at Texas by DARPA/ARO and DoD/MURI.

[1] J. P. Liu, Y. Liu, C. P. Luo, Z. S. Shan, and D. J. Sellmyer, J. Appl. Phys. **81**, 5644 (1997).
[2] S. Sun, C. B. Murray, D. Weller, L. Folks, and A. Moser, Science **287**, 1989 (2000).
[3] H. Zeng, J. Li, J. P. Liu, Z. L. Wang, and S. H. Sun, Nature (London) **420**, 39 (2002).
[4] S. Okamoto, O. Kitakami, N. Kikuchi, T. Miyazaki, Y. Shimada, and Y. K. Takahashi, Phys. Rev. B **67**, 094422 (2003).
[5] C. B. Rong, H. W. Zhang, X. B. Du, J. Zhang, S. Y. Zhang, and B. G. Shen, J. Appl. Phys. **96**, 3921 (2004).
[6] J. W. Harrell, S. Kang, Z. Jia, D. E. Nikles, R. Chantrell, and A. Satoh, Appl. Phys. Lett. **87**, 202508 (2005).
[7] J. M. Qiu, J. M. Bai, and J. P. Wang, Appl. Phys. Lett. **89**, 222506 (2006).
[8] C. B. Rong, D. R. Li, V. Nandwana, N. Poudyal, Y. Ding, Z. L. Wang, H. Zeng, and J. P. Liu, Adv. Mater. (Weinheim, Ger.) **18**, 2984 (2006).
[9] C. B. Rong, N. Poudyal, G. S. Chaubey, V. Nandwana, R. Skomski, Y. Q. Wu, M. J. Kramer, and J. P. Liu, J. Appl. Phys. **102**, 043913 (2007).
[10] R. A. Ristau, K. Barmak, L. H. Lewis, K. R. Coffey, and J. K. Howard, J. Appl. Phys. **86**, 4527 (1999).
[11] O. N. Mryasov, U. Nowak, K. Y. Guslienko, and R. W. Chantrell, Europhys. Lett. **69**, 805 (2005).
[12] J. Zhou, R. Skomski, K. D. Sorge, and D. J. Sellmyer, Scr. Mater. **53**, 455 (2005).
[13] K. Elkins, D. Li, N. Poudyal, V. Nandwana, Z. Jin, K. Chen, and J. P. Liu, J. Phys. D **38**, 2306,(2005).
[14] W. F. Brown, *Micromagnetics* (Wiley, New York, 1963).
[15] R. Skomski, J. Phys.: Condens. Matter **15**, R841 (2003).
[16] R. Skomski, J. P. Liu, and D. J. Sellmyer, Phys. Rev. B **60**, 7359 (1999).
[17] R. Skomski and J. M. D. Coey, Phys. Rev. B **48**, 15812 (1993).
[18] H. Kronmüller, Phys. Status Solidi B **144**, 385 (1987).
[19] *Handbook of Mathematical Functions*, edited by M. Abramowitz and M. I. Stegun (Dover, New York, 1965).